

Computational Simulation of Duplex Stainless Steel Continuous Cooling Transformation Curves Using DICTRA®

Rayanne Araujo Andrade^{a*} , Rodrigo Magnabosco^a 

^aCentro Universitário da Fundação Educacional Inaciana “Padre Sabóia de Medeiros” (FEI),
Departamento de Engenharia de Materiais, São Bernardo do Campo, SP, Brasil.

Received: November 22, 2021; Revised: February 01, 2022; Accepted: February 04, 2022

Despite of their excellent combination of high mechanical strength, toughness and corrosion resistance, duplex stainless steels (DSS) are susceptible to sigma phase formation, negatively affecting their superior properties. Sigma formation continuous cooling transformation (CCT) diagrams can be a useful tool to avoid sigma formation during cooling from solution treatment temperatures; however, non-isothermal information about sigma formation in DSS are scarce in literature. This work presents a methodology to simulate CCT diagrams in DICTRA® software, showing excellent adherence to literature data. The methodology here presented was also able to describe sigma phase formation behaviour for different DSS compositions.

Keywords: *Computation simulation, stainless steel, sigma phase, CCT, DICTRA.*

1. Introduction

Duplex stainless steels (DSS) are largely used in industrial equipment that need the combination of high mechanical strength, toughness, and corrosion resistance, such as the ones found in chemical and petrochemical plants, pulp and paper industries, offshore structures and machinery, and desalinization plants. The desired properties were obtained through an ideal microstructure consisted of approximately equal amounts of ferrite (α) and austenite (γ), both with high amounts of Cr, Mo, and N, after a solution treatment between 1000 °C and 1200 °C¹⁻⁵.

Cooling from solution treatment temperatures were conducted at high cooling rates, since undesirable phase formation can occur in the temperature range from 1000 °C to 600 °C⁶. The most deleterious phase formed in this temperature range is sigma, due to the large amounts of Cr and Mo in its composition, causing impoverishment of those elements, which are essential to a proper passive film formation^{7,8}. Sigma phase, characterized by a brittle behaviour, is also responsible for loss of toughness, leading to brittle fracture of components, even if only small amounts of sigma are formed^{9,10}. Development of higher Cr and Mo DSS, creating the so-called superduplex or hyperduplex stainless steels for even higher corrosion resistance in the solution-treated condition, worsens the problems involving sigma formation, since higher amounts of Cr and Mo facilitate nucleation and growth of sigma^{11,12}.

Kinetics of sigma phase formation, specially using models based in Kolmogorov-Johnson-Mehl-Avrami (KJMA) equation, can be found in literature¹³⁻¹⁶, allowing the creation of isothermal Time-Temperature-Precipitation (TTP) diagrams of sigma formation in DSS. However, when cooling from the solution temperature is the key to avoid sigma formation, TTP diagrams are not the best instrument of analysis, being

the continuous cooling transformation (CCT) diagrams the most indicated feature. However, literature has rare examples of non-isothermal formation of sigma, probably due to the difficulty of obtaining experimental data¹⁵⁻¹⁹.

One alternative to the experimental data on sigma phase formation under non-isothermal conditions is the computational simulation. Thermo-Calc® and DICTRA® showed promising results describing, respectively, equilibrium of phases and diffusion-controlled transformations of DSS^{18,20-23}.

This work studied sigma phase formation in different DSS compositions under different continuous cooling rates from solution treatment temperatures, developing a methodology for creating sigma phase formation CCT diagrams using DICTRA® software, and validating it with literature results.

2. Methodology

Three DSS compositions were chosen for modelling using Thermo-Calc® and DICTRA®, as presented in Table 1, characterizing the most important basic compositions related to corrosion resistance: duplex, superduplex and hyperduplex stainless steels, that were based on from the literature data^{8,10,14,23-25}. As can be seen in Table 1, the hyperduplex grade has the highest Cr, Mo, and N contents.

Thermo-Calc® equilibrium simulation was performed, using TCFE9 as thermodynamic database, to obtain the temperature where only ferrite and austenite are present, in equal volume fractions, characterizing the ideal solution-treatment temperature. Chemical composition of ferrite (α) and austenite (γ) in this solution-treatment temperature (T_s) can be found in Table 2.

DICTRA® simulations described phase transformations during cooling from T_s temperatures (Table 2) under several cooling rates, from 0.001 to 100°C/s. Thermodynamic data needed for local equilibrium simulations were provided by

*e-mail: rayanneaa@hotmail.com

Table 1. Chemical composition of the studied materials.

Element [mass %]	%Cr	%Mo	%Ni	%N	%Fe
Duplex	22.0	5.0	3.0	0.17	Balance
Superduplex	25.0	7.0	4.0	0.3	Balance
Hyperduplex	27.0	7.0	4.8	0.4	Balance

Table 2. Composition of ferrite (α) and austenite (γ), and the solution-treatment temperature (T_s) for each studied material.

Material	phase	%Cr	%Mo	%Ni	%N	T_s [°C]
Duplex	α	23.6	3.76	3.68	0.025	1041
	γ	20.4	6.23	2.32	0.320	
Superduplex	α	26.2	5.49	4.87	0.053	1141
	γ	23.8	3.13	8.51	0.548	
Hyperduplex	α	27.7	5.47	5.86	0.051	1107
	γ	26.3	8.53	3.73	0.750	

TCFE9 database, and mobility data were obtained in MOBFE4 database. Planar and unidirectional diffusion flux model was created, constituted by a ferrite cell placed at the right side of an austenite cell. Sigma, inactive in the beginning of simulation, can be formed in the ferrite-austenite interface when a thermodynamic potential for sigma formation of 10^{-5} RT was reached, being R the universal gas constant (8.314 J/mol K) and T the absolute temperature in [K]. Each phase cell has an initial size of 50 μm , and 100 points per phase cell, placed in a geometric distribution along the cell length, allowing a large numbers of calculation points in the vicinity of the ferrite-austenite interface, where sigma will be formed. Figure 1 presents a schematic representation of the computational cell.

Sigma definition in both TCFE9 and MOBFE4 databases did not consider nitrogen as a constituent. For this reason, DICTRA[®] simulations were divided in two steps. This is necessary considering that between T_s and the maximum temperature where sigma is possible in a DSS (T_σ^c , exemplified in the equilibrium diagram plotted in Figure 2) ferrite and austenite are the only phases present, and all alloying elements must be partitioning between them, influencing volume fraction of phases and their compositional gradients. A first step in simulation must consider all alloying elements, including N, at least between T_s and T_σ^c .

However, even below T_σ^c , thermodynamic potential for sigma formation may not be reached, and an undercooling below T_σ^c was necessary to reach the desired thermodynamic potential for sigma formation. To estimate the temperature, below T_σ^c , where the sigma phase formation starts, initially in DICTRA[®] a pre-simulation was performed without nitrogen in the chemical composition of the phases, to identify at which temperature there is thermodynamic potential for the formation of the sigma phase at the austenite-ferrite interface, a temperature called T_σ . This simulation is performed in a single step, starting at the solution temperature presented in Table 2 up to 741°C. Values of T_σ^c (determined in equilibrium diagrams like the one in Figure 2) and T_σ (determined in this pre-simulation step) for the duplex stainless steels here studied are found in Table 3.

Knowing the temperature at which the sigma phase would precipitate during cooling (T_σ) the first step of cooling in proposed simulation model happens from T_s to T_σ . In this first step, nitrogen is present with the other elements

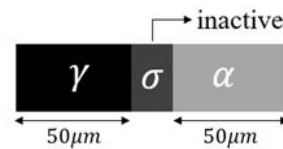


Figure 1. schematic representation of the computational cell, where austenite (γ) is placed at the left of the model, ferrite (α) at the right, and sigma (σ , inactive in the beginning of simulation, only formed after a thermodynamic potential for sigma formation of 10^{-5} RT was reached).

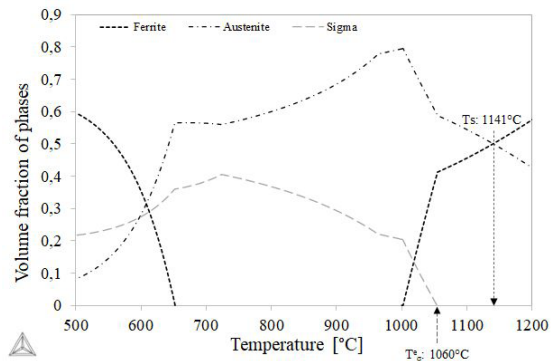


Figure 2. Equilibrium diagram for the studied superduplex stainless steel obtained in Thermo-Calc[®] (TCFE9 database), showing ideal solution treatment temperature (T_s) and the maximum temperature where sigma is possible (T_σ^c)

in a linear function, corresponding to the partition of the elements between the ferrite and austenite phases, at T_s temperature. At the end of the first step, when T_σ is reached, computational cell size and the composition gradients of the elements on ferrite and austenite phases are extracted, to be used as initial conditions for the second step of cooling, which takes place from T_σ temperature up to 741°C. In this temperature range sigma phase precipitates, so nitrogen is not added to the chemical composition of the phases. This methodology was called “2-step methodology”. Figure 3 presents a schematic representation of the thermal cycles and simulations performed in the 2-step methodology here proposed. In Figure 3a, pre-simulation for estimation of T_σ is described, without N in chemical composition of

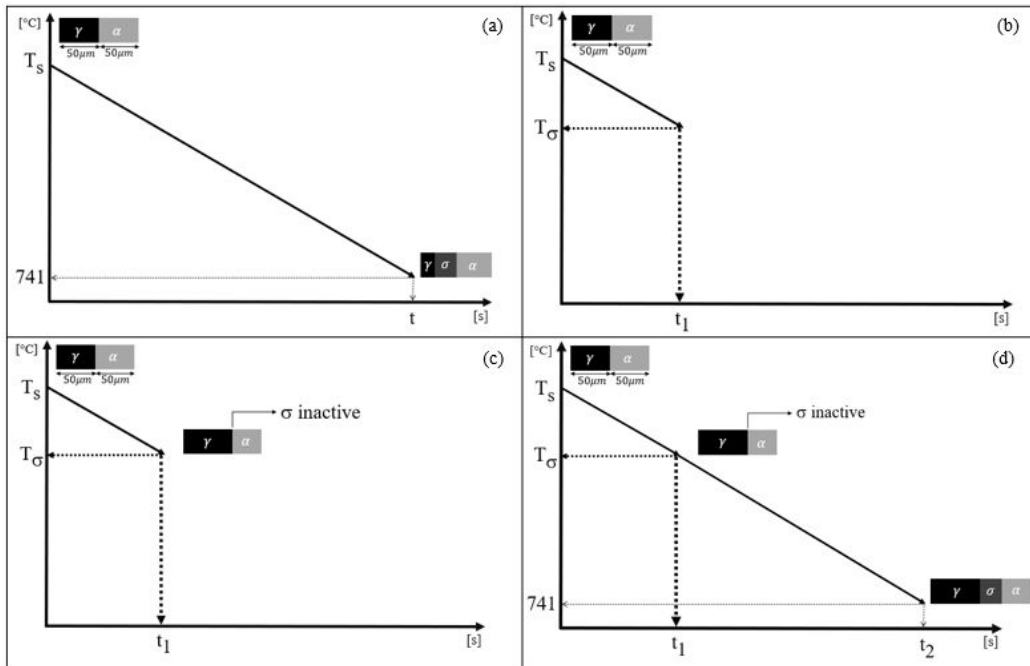


Figure 3. Schematic representation of the 2-step methodology: (a) pre-simulation; (b) first step, including N, to allow partitioning of alloying elements between ferrite (α) and austenite (γ); (c) determination of equilibrium between α and γ at T_σ ; (d) second step, without N, allowing σ formation at α - γ interface.

Table 3. T_σ^c and T_σ for the studied alloys.

	Duplex	Superduplex	Hyperduplex
T_σ^c [°C]	961	1060	1097
T_σ [°C]	941	1030	1060

phases. First step of the model is represented in Figure 3b, determining the time t_1 at a specific cooling rate to reach T_σ in a system where all alloying elements of Table 2, including N, can be partitioning between ferrite and austenite. At t_1 , composition gradients of ferrite and austenite cells (excluding N), and volume fractions of these phases, became the initial conditions for the second step of the model, where sigma is allowed to form in ferrite-austenite interface. The end of the second step is represented in Figure 3d, where time t_2 where obtained, in the same cooling rate imposed in the other steps described.

At the end of the 2-step methodology, for each cooling rate, it is possible to create a diagram as exemplified in Figure 4. The construction of CCT diagram for a specific volume fraction of sigma formed during cooling demands the sum of time t_1 from the first step (Figure 3c) and the time for formation of 1%vol of sigma, $t_{\sigma,1\%}$ defined in Figure 4. In a specific cooling rate, the sum of t_1 and $t_{\sigma,1\%}$ define the time at that cooling rate when 1% of sigma will be formed. This time, and the temperature at which $t_{\sigma,1\%}$ was defined, are the coordinates of one point of the CCT curve for 1% sigma formation.

3. Results and Discussion

Figure 5 shows Cr composition profiles at the α - γ interface for the superduplex alloy at a cooling rate of 0.001°C/s. Each

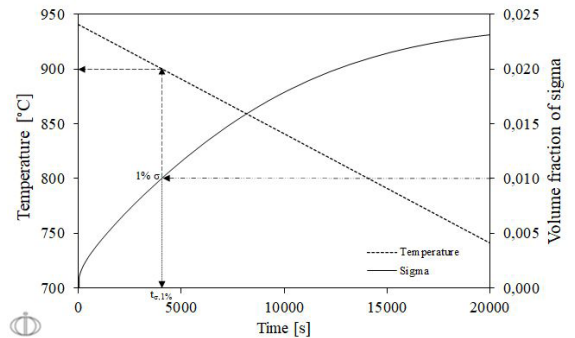


Figure 4. Temperature and volume fraction of sigma as a function of time for cooling rate of 0.01 °C/s in a duplex stainless steel after second step of the proposed methodology.

line of the diagrams represents the composition profile for a given time, the solid line, $t = 0$, shows the composition profile at time zero, so it is the initial linear composition of Table 2 for both phases. With the progress of cooling the composition profile changes and when the sigma phase precipitates Cr concentration increases to approximately 32%, which is the expected Cr content of sigma phase. Figure 5a is a result from the pre-simulation step, where N was not considered as phases constituent, and the reduction of austenite content with increasing time (or reduction in temperature during cooling), characterized by the shift to the left of the austenite-ferrite interface, can be observed: this non-expected behaviour is due to the absence of N, and the consequent odd partition of alloying elements between ferrite and austenite. Since N is an element notably known as austenite stabilizer, its absence leads to a decrease in

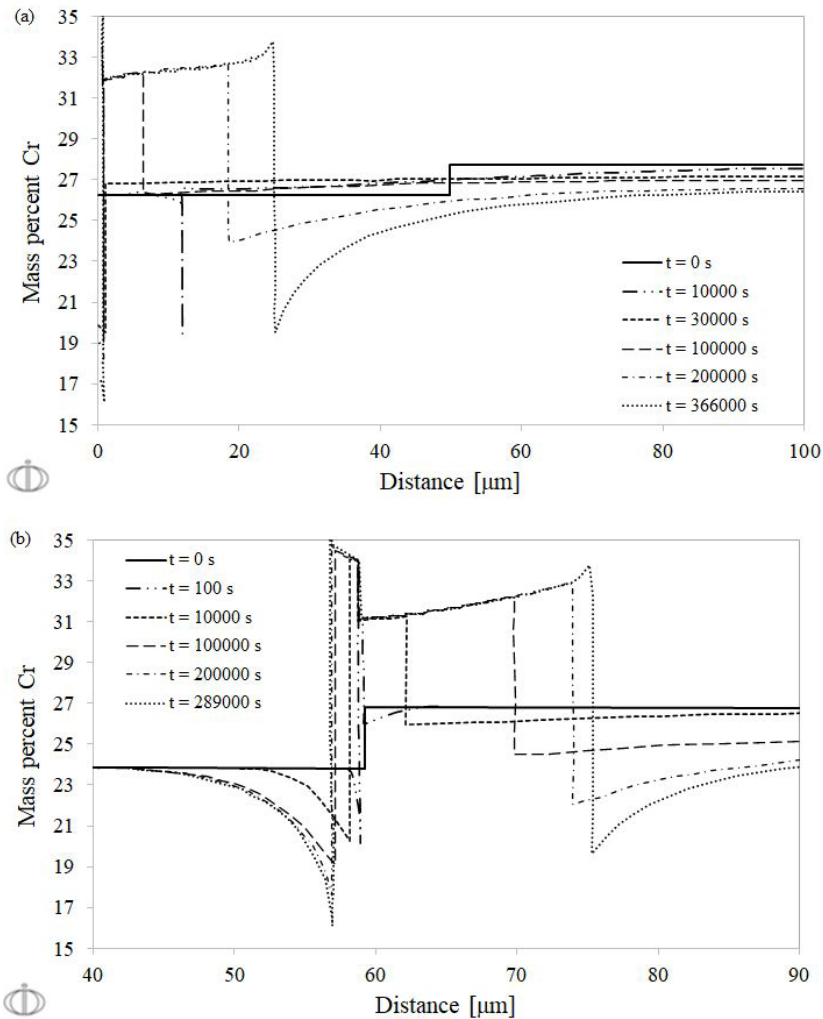


Figure 5. Cr profiles during sigma formation in the studied superduplex stainless steel during cooling at 0.001°C/s from T_s temperature (a) or T_{σ} temperature (b). In (a), the pre-simulation stage, N was not considered in DICTRA[®] simulation. (b) is the second step of the “2-step methodology” here proposed.

the fraction of this phase, and an increase in the fraction of ferrite, even with the reduction in temperature, a fact that is not expected by the phase equilibrium, as already shown in Figure 2.

The 2-step methodology proposed did not allow the reduction on ferrite content, as presented in Figure 5b. The presence of N in the first step stabilized austenite, allowing the correct partitioning of alloying elements between ferrite and austenite between T_s and T_{σ} . Since composition profiles of all times in Figure 5b (except for time $t=0$, presented only to mark the position of the initial α - γ interface) are related to the second step of simulation, it is possible to detect sigma formation in 100 s of simulations at that cooling rate, with reduction of ferrite content to allow sigma formation, as previously observed by Morais and Magnabosco²². Cr-impoverishment at γ - σ and σ - α interfaces can also be observed, in accordance with other work²³ that related these Cr-depleted areas to loss of localized corrosion resistance.

The importance of the 2-step methodology here proposed can be verified in Figure 6, which presents CCT diagrams

for the hyperduplex composition of Table 1, calculated with the results of the pre-simulation stage (without N in the composition) and the 2-step methodology. The higher ferrite content obtained in the pre-simulation stage, as consequence of the odd partitioning of alloying elements, lead to a ferrite prior to sigma formation with smaller amounts of sigma forming elements Cr and Mo, which are diluted in this higher amount of ferrite formed. With this, pre-simulation results lead to a slower sigma formation kinetics, and the CCT curves of this pre-simulation are to the right of those of the 2-step methodology.

The 2-step methodology was then applied to the compositions of typical duplex, superduplex and hyperduplex stainless steels (Table 1), enabling the construction of CCT diagrams for 1%vol of sigma, as presented in Figure 7. It was found that higher Cr and Mo contents shift the CCT curves to the left, accelerating the sigma phase formation kinetics, as these elements increase the thermodynamic potential for sigma phase formation. Thus, it can be concluded that the use of 2-step methodology in DICTRA[®] software describes

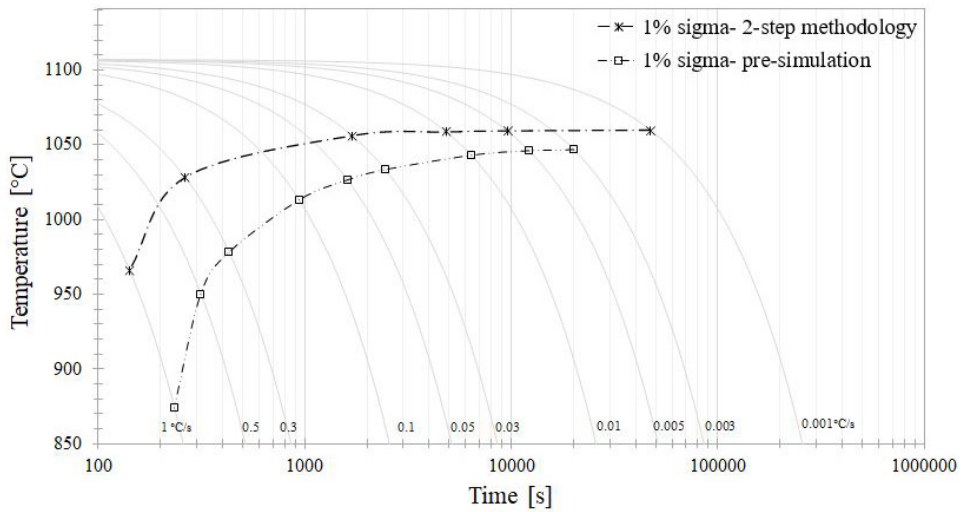


Figure 6. Hyperduplex stainless steel CCT diagrams for 1%vol sigma obtained with pre-simulation or 2-step methodology results.

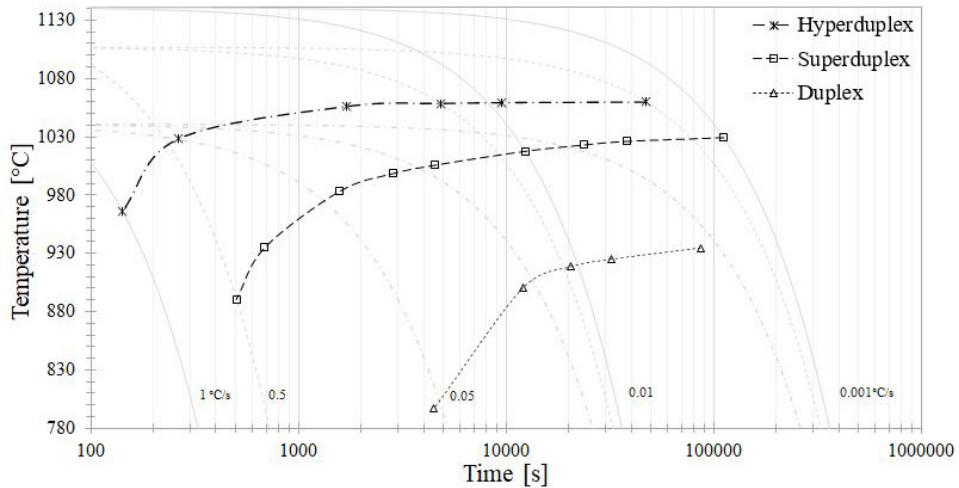


Figure 7. CCT diagrams of 1%vol sigma for different DSS using the 2-step methodology.

microstructural behaviours consistent with observed in literature^{10,12,15,17,18}.

In Figure 7 the size of each phase in the computational cell at the beginning of the first step was maintained in 50 μm . However, the size of the phases in the model did affect results, as presented in Figure 8. Reduction in the size of the computational cell shifts CCT diagrams to the left, accelerating the sigma phase formation kinetics. This may be a result of the increase in the concentration gradient of the elements, making the thermodynamic potential for the formation of the sigma phase greater. Similar results were reported by Pardal et al.²⁴: authors correlate the increase in sigma phase formation to the reduction in grain size, which can be related to the size of the phases in the computational cell. However, Pardal et al.²⁴ associated the smaller grain size to an increase in the number of heterogeneous nucleation sites, a factor that has a strong impact on sigma phase precipitation, as also reported by Melo and Magnabosco²⁶. In DICTRA® software, the computational model is made of a single ferrite/austenite

interface, without considering the number of nucleation sites, and there is no viable conclusion regarding nucleation sites. DICTRA® results here presented indicates that the sigma phase formation may indeed have a strong diffusional control component, as reported in previous works^{13,14}. Considering those facts, the size of the phases in the computational cell is another key initial value for the simulations.

The 2-step methodology proposed here was applied to the experimental data provided by Ferro and Bonollo¹⁷, which quantified sigma content obtained after continuous cooling of a DSS. The chemical composition of the steel was used in Thermo-Calc® with TCFE9 database, for determination of the initial austenite and ferrite reported, and the equilibrium compositions of these phases at the ideal solution treatment temperature. Those results are the initial conditions used in the 2-step methodology in DICTRA®, using TCFE9 and MOBFE4 databases. Information from the work¹⁷ that the average grain size was 20 μm was used as initial size for ferrite and austenite in the computational cell^{18,27}. CCT curve

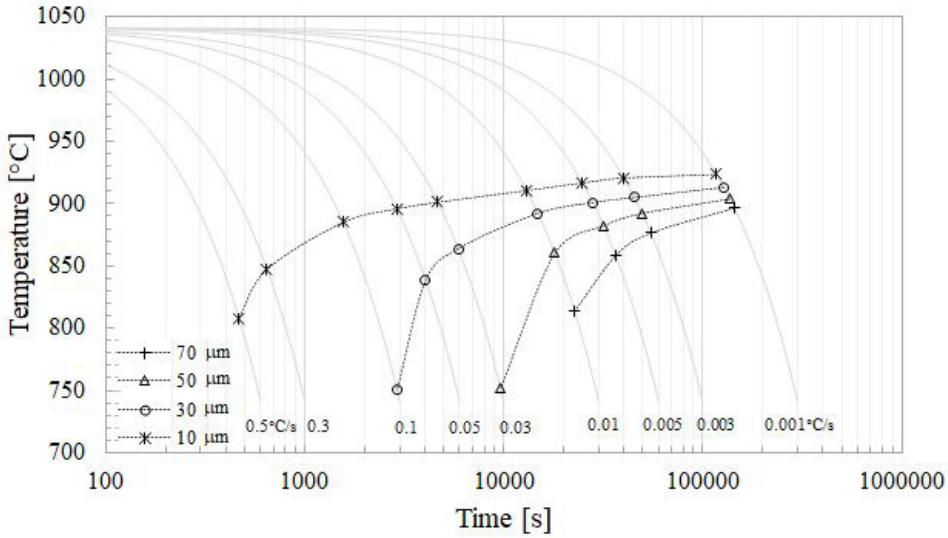


Figure 8. CCT curves of a DSS for 1%vol sigma for different initial sizes of ferrite or austenite in the computational cell.

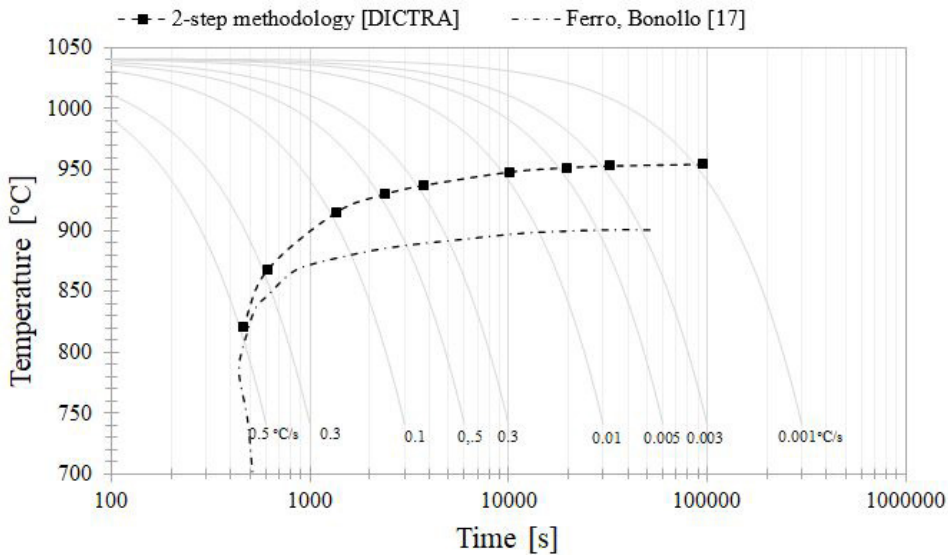


Figure 9. CCT curve for 1%vol sigma of a DSS obtained experimentally [17] compared to the simulated by the 2-step methodology here proposed.

obtained in the 2-step methodology and the experimental curve from Ferro and Bonollo¹⁷ are compared in Figure 9. It can be noted that critical cooling rate to avoid sigma formation declared in¹⁷, between 0.3 °C/s and 0.7 °C/s, is in good agreement to the one obtained in DICTRA[®] using the 2-step methodology, which was 0.5 °C/s. It is important to note that cooling rates between 0.25 °C/s and 1°C/s can result in very small amounts of sigma^{25,28}, and experimental results can be very influenced by experimental imprecisions during quantification, or difficulties in ensuring the representativeness of the sample with the fields analysed in sigma quantification¹⁷.

Therefore, the methodology proposed here can be a viable alternative, as it allows the evaluation of modification

of the chemical composition, solution treatment temperature and computational cell size, simulating for different systems different CCT curves for a specific condition. This will be much easier than the experimental method of trial and error seeking to reproduce experimentally the behavior of DSS concerning the formation of the sigma phase in non-isothermal conditions, and consequently helping in real production processes.

4. Conclusions

1. The 2-step methodology here proposed using DICTRA[®] software is capable of reproducing sigma phase formation curves during continuous cooling, and microstructures such as those in the literature.

By adding the parameters of chemical composition, solution-treatment temperature, and computational cell size, it is possible to study the formation of the sigma phase during cooling for different DSS.

2. Performing a pre-simulation without N to obtain the temperature where there is thermodynamic potential for sigma formation in DSS is essential to describe the correct fraction of ferrite and austenite before sigma phase formation during cooling from the solution treatment temperature, and the correct alloying element partition gradients between ferrite and austenite before sigma phase formation.
3. Computational cell size showed great influence on sigma phase precipitation during cooling from solution treatment temperature of DSS, as with cell size reduction there is an increase in the concentration gradient, favoring sigma phase formation.

5. References

1. Verma J, Taiwade RV. Effect of welding processes and conditions on the microstructure, mechanical properties and corrosion resistance of duplex stainless steel weldments: a review. *J Manuf Process.* 2017;25:134-52.
2. Zou D, Han Y, Zhang W, Junhui Y. Sigma phase precipitation and properties of super-duplex stainless steel UNS S32750 aged at the nose temperature. *Mater Sci.* 2011;26:182-5.
3. Zhang Z, Zhao H, Zhang H, Hu J, Jin J. Microstructure evolution and pitting corrosion behavior of UNS S32750 super duplex stainless steel welds after short-time heat treatment. *Corros Sci.* 2017;121:22-31.
4. Zhang B, Wei XX, Wu B, Wang J, Shao XH, Yang LX, et al. Chloride attack on the passive film of duplex alloy. *Corros Sci.* 2019;154:123-8.
5. Lothongkum G, Wongpanya P, Morito S, Furuahara T, Maki T. Effect of nitrogen on corrosion behavior of 28Cr–7Ni duplex and microduplex stainless steels in air-saturated 3.5 wt% NaCl solution. *Corros Sci.* 2006;48:137-53.
6. Wang R. Precipitation of sigma phase in duplex stainless steel and recent development on its detection by electrochemical potentiokinetic reactivation: a review. *Corrosion Communications.* 2021;2:41-54. <https://doi.org/10.1016/j.corcom.2021.08.001>.
7. Tan H, Jiang Y, Deng B, Sun T, Xu J, Li J. Effect of Annealing temperature on the pitting corrosion resistance of super duplex stainless steel UNS S32750. *Mater Charact.* 2009;60:1049-54.
8. Sun L, Sun Y, Liu Y, Dai N, Liu J, Jiang Y. Effect of annealing temperature on pitting behavior and microstructure evolution of hyper-duplex stainless steel 2707. *Mater. Corros.* 2019;51:1-11.
9. Biezma MV, Martin U, Linhardt P, Röss J, Rodrigues C, Bastidas DM. Non-destructive techniques for the detection of sigma phase in duplex stainless steel: a comprehensive review. *Eng Fail Anal.* 2021;122:105227.
10. Kim YL, Chumbley LS, Gleeson B. Continuous cooling transformation in cast duplex stainless steels CD3MN and CD3MWCuN. *J Mater Eng Perform.* 2008;17:234-9.
11. Chai G, Kangas P. Super and Hyper Duplex Stainless Steels: structures, properties and applications. *Procedia Structural Integrity.* 2016;2:1755-1762.
12. Keplinger A, Martinez C, Hausbauer M, Kapp M. Early stages of deleterious phase in super and hyper duplex stainless steel and their effect on toughness. *Berg- Huetttenmaenn. Monatsh.* 2020;165:33-9.
13. Magnabosco R. Kinetics of sigma phase formation in a Duplex Stainless Steel. *Mater Res.* 2009;12:321-7.
14. Santos DC, Magnabosco R. Kinetic study to predict sigma phase formation in Duplex Stainless Steels. *Metall Mater Trans, A Phys Metall Mater Sci.* 2016;47A:1554-65.
15. Byun S-H, Kang N, Lee T-H, Ahn S-K, Lee HN, Chang W-S, et al. Kinetics of Cr/Mo-rich precipitates formation for 25Cr-6.9Ni-3.8Mo-0.3N Super Duplex Stainless Steel. *Met Mater Int.* 2012;18:201-7.
16. Zhang B, Jiang Z, Li H, Zhang S, Feng H, Li H. Precipitation behavior and phase transformation of Hyper Duplex Stainless Steel UNS S32707 at nose temperature. *Mater Charact.* 2017;129:31-9.
17. Ferro P, Bonollo F. A semiempirical model for sigma-phase precipitation in duplex and superduplex stainless steels. *Metall Mater Trans, A Phys Metall Mater Sci.* 2012;43A:1109-16.
18. Wessman S, Pettersson R. Application of computational thermodynamics to predict growth of intermetallic phases in Super Duplex Stainless Steels. *Steel Res Int.* 2015;86:1339-49.
19. Freitas GCLD, Fonseca GS, Moreira LP, Leite DNF. Phase transformation of the duplex stainless steel UNS S31803 under non-isothermal conditions. *J. Mater. Res. Technol.* 2021;11:1847-51.
20. Li J-B, Yang C, Dong H. Computer simulations of phase transformation in steels. *Mater Des.* 2001;22:39-43.
21. Malik A, Odqvist J, Hoglund L, Hertzman S, Agren J. Phase-field modelling of sigma-phase precipitation in 25Cr7Ni4Mo duplex stainless steel. *Metall Mater Trans, A Phys Metall Mater Sci.* 2017;48A:4914-28.
22. Morais LC, Magnabosco R. Experimental investigations and DICTRA® simulation of sigma phase formation in a duplex stainless steel. *Calphad.* 2017;58:214-8.
23. Magnabosco R, Morais LC, Santos DC. Use of compositions profiles near sigma phase for assessment of localized corrosion resistance in a duplex stainless steel. *Calphad.* 2019;64:126-30.
24. Pardal JM, Tavares SS, Fonseca MC, Souza JA, Côte RAA, Abreu HFG. Influence of the grain size on deleterious phase precipitation in superduplex stainless steel UNS S32750. *Mater Charact.* 2009;60:165-72.
25. Sieurin H, Sandstrom R. Austenite reformation in the heat-affected zone of duplex stainless steel 2205. *Mater Sci Eng A.* 2006;419:250-6.
26. Melo EA, Magnabosco R. Magnabosco, Influence of the heterogeneous nucleation sites on the kinetics of intermetallic phase formation in aged duplex stainless steel. *Metall Mater Trans, A Phys Metall Mater Sci.* 2017;48A:5273-84.
27. Wessman S. On the use of computational thermodynamics for predicting the precipitation and growth of secondary phases in stainless steels. In: 10th European Stainless Steel Conference; 2019 Sep 3-Oct 2; Vienna. Proceedings. Vienna: Austrian Society for Metallurgy and Materials (ASMET); 2019.
28. Chiu LH, Hsieh WC, Wu CH. Colling rate effect on vacuum brazed joint properties for 2205 Duplex Stainless Steels. *Mater Sci Eng A.* 2003;354:82-91.